Colloid Polym Sci 275:407–418 (1997)

ORIGINAL CONTRIBUTION

E. Cappelaere
R. Cressely

Shear banding structure in viscoelastic micellar solutions

Received: 4 July 1996
Accepted: 19 November 1996

E. Cappelaere · Prof. R. Cressely (✉)
Institut de Physique
Laboratoire de Physique des Liquides
et des Interfaces
Groupe Rhéophysique des Colloides
Université de Metz
1 Bd. F. Arago
57078 Metz Cedex 3, France

Abstract Theoretically, it has been shown that worm-like micellar solutions of surfactant can, for a shear rate $\dot{\gamma}$ greater than a critical value $\dot{\gamma}_c$, undergo a transition giving a plateau evolution ($\sigma = \sigma_c$) of the shear stress σ against shear rate $\dot{\gamma}$. We report here on a experimental study of the linear and nonlinear rheological behaviour of aqueous CTAB solutions with $NaNO_3$ as added salt. With this system, it is possible to observe the evolution of the fundamental characteristics of the flow curve, i.e., the shear rate $\dot{\gamma}_{1c}$ at which a shear banding structure appears and the second critical shear rate $\dot{\gamma}_{2c}$ characterizing the end of the shear stress plateau followed by a new increased shear stress. For the first time, experimentally, we obtained evidence for the existence and the evolution of $\dot{\gamma}_{2c}$ against CTAB and salt concentrations and temperature variations. Experimental results are compared to theoretical predictions correlating σ_c, $\dot{\gamma}_{1c}$ and G_0 (the shear modulus) for Maxwellian micellar solutions.

Key words Rheological – micellar – CTAB – $NaNO_3$ – shear banding

Introduction

The size, shape and organisation of surfactant micelles usually depend on the temperature, the nature and concentrations of surfactant and salt (if salt is added). Studies of ionic surfactants in water show that detergent molecules in some systems assemble reversibly into flexible worm-like micelles that can form a viscoelastic fluid. It has been shown that some rheological properties of semi-dilute solutions of such micellar systems are very similar to the properties of entangled conventional polymer [1–4]. A fundamental difference however is that, contrary to ordinary polymers, the micellar chains are equilibrium objects: they can reversibly break and recombine (they are often called "living polymers"). The living character of the micelles provides additional pathways for disentanglement. This property has crucial consequences on their rheological behaviour, especially in the nonlinear regime.

The micellization of ionic surfactant eventually followed by the elongation of the micelles, in aqueous solutions, results with increasing concentration, from a complex balance between the hydrophobic interaction of the detergent molecules and electrostatic interaction (between their ionic head coupled with the electrostatic action of the counterions). Addition of salt increases the screening of the surface charges, reduces the electrostatic repulsions and so facilitate aggregation. The specificity of some counterions to induce the elongation of CPX or CTAX micelles in aqueous solution has been investigated experimentally [5]. It has been shown that Br^-, NO_3^-, ClO_3^- promote their elongation with increasing efficiency from Br^- to ClO_3^-. F^- as well as Cl^- were found inefficient in promoting the elongation.

Hexadecyltrimethylammonium bromide (CTAB) is one of the most popular cationic surfactant system studied during the past years. For example, semidilute aqueous solutions of CTAB in the presence of potassium bromide

Colloid & Polymer Science, Vol. 275, No. 5 (1997)

KBr have been extensively studied [1, 2, 6]. In this experimental study we work with CTAB with sodium nitrate ($NaNO_3$) as an added salt, NO_3^- being more efficient than Br^- in promoting the elongation of the micelle. Using ion-specific electrode, Larsen and Magid [7] showed NO_3^- to displace Br^- from micelles in CTAB solutions. With appropriate concentration with this system, as we can see later, we can obtain viscoelastic solutions with flexible worm-like micelles.

To describe the rheological properties of these surfactant systems, a model based on the tube model (reptation) of polymer dynamics, including the effects of reversible breaking, has been proposed by Cates [8]. The behaviour in the linear regime is well understood. It depends on the relative value of the breaking time τ_b of the micelle and of τ_{rep}, the reptation time of a polymeric micelle with a length equal to average micellar length $\bar{L}$.

When τ_b is large compared to τ_{rep} ($\tau_b \gg \tau_{rep}$), the breaking mechanism is not important for stress relaxation, and consequently the theory of reptation of ordinary polydisperse polymer should apply. As a result the stress relaxation function is strongly non-monoexponential.

If $\tau_b \ll \tau_{rep}$, Cates' model predict an almost pure exponential form of the stress relaxation with a terminal relaxation time τ_R given by $\tau_R = (\tau_b \tau_{rep})^{1/2}$. For the zero shear viscosity η_0 we have the relation $\eta_0 = G_0 \tau_R$ where G_0 is the plateau modulus. When the micelles in solution are entangled (a condition of application of this theory), experimental results are often in agreement with Cates' predictions [9].

The dynamic behaviour of complex fluid like surfactant solutions in the non-linear regime is more complex, yet it has been the subject of intensive theoretical and experimental research in recent years. The rheological response results then, for sufficiently great values of the shear rate $\dot{\gamma}$, from non-equilibrium systems. Theoretically, the non-linear response of a material is governed by its constitutive equation. A constitutive scheme for reversibly breakable chain was proposed by Cates [8] and has been studied numerically by Spendley et al. [10]. The deformation is postulated to be not so large as to cause mechanical rupture of the micelles. For steady flow, the constitutive equation can be solved numerically. The model predicts a Newtonian first domain (I), in which the shear stress σ increase linearly with the shear rate $\dot{\gamma}$ up to $\sigma = \sigma_c = 0.67 G_0$, obtained for a critical shear rate $\dot{\gamma}_{1c} = 2.6/\tau_R$. Then, the predicting decreasing shear stress at $\dot{\gamma} > \dot{\gamma}_{1c}$ suggests that the steady shear flow in this region is unstable so giving a shear banding structure. In this domain, (II), practically, the shear stress saturates to a constant value σ_c. For $\dot{\gamma}$ greater than a second critical value $\dot{\gamma}_{2c}$, eventually there must be an upturn at flow rates beyond the range for which the model applies. The evolution of $\sigma(\dot{\gamma})$ is schematically represented in Fig. 1. The last part of the curve (domain III) is only speculative in this theory. It can be noticed that in steady shear flow for $\dot{\gamma}_{1c} < \dot{\gamma} < \dot{\gamma}_{2c}$ (when $\dot{\gamma}$ is increasing) the shear banding structure consist of two or more "shear bands". These are layers of high and low shear rate material (but same shear stress) which co-exist at a volume fraction arranged to match the imposed macroscopic shear rate.

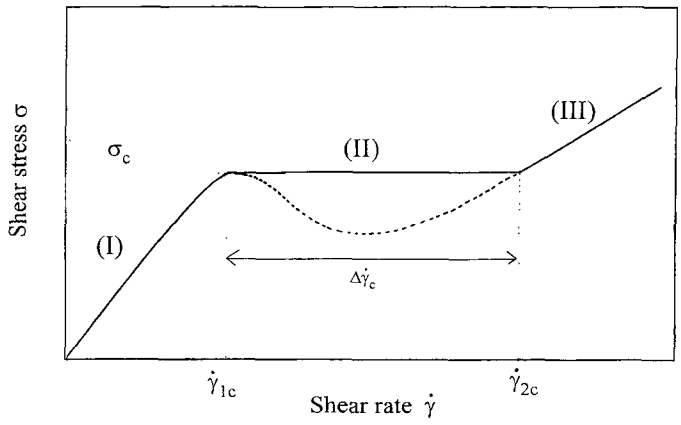

Fig. 1 Schematic steady shear stress/shear rate curves. The dotted line corresponds to theoretical predictions according to [18, 28]. Decreasing of shear stress induce instabilities of the shear banding type

In this experimental work, we present the experimental results obtained with CTAB and $NaNO_3$ as an added salt. With this system we can observe the three parts of the stress/rate curve and we compare the characteristic experimental values obtained with theoretical predictions of the Cates' model.

Experimental

Our study is carried out on aqueous CTAB solutions with $NaNO_3$. The CTAB (surfactant) product and the salt are commercially available (Acros Organics). The solutions studied here were prepared at surfactant concentrations higher than c^* (concentration above which the micelles start to overlap). The solvent is pure water distilled twice in a quartz vessel. Special devices were used to avoid evaporation. Standard procedures, described in a previous work [11], were used to prepare the solutions which were left to stand at rest at least for three days in order to reach equilibrium.

The rheological measurements presented here were all performed with the Carrimed CSL 100 working in the constant shear stress mode and using different cone plane devices which lead to a wide range of shear rate (generally

the shear rate could be varied from 1 to 6000 s^{-1} approximately). This apparatus allows viscosity measurements to be taken at sufficiently low and high shear rates to get the zero shear rate viscosity η_0 and the non-Newtonian range. The sample is studied in a temperature range which is above the Kraft temperature of the solution. All the results reported in this paper correspond to experiments at the end of which the solution was apparently in a perfect state and which are, for the same experimental conditions, reproducible. The samples were generally studied in the temperature range 30–48 °C. The fresh surfactant solutions as well as the solutions which were submitted to shearing stress during an experiment, were completely transparent and free from foam and air bubbles. In order to allow for a significant comparison of the experimental results, all the measurements were rigorously performed with the same procedure. For each experiment we have used a new sample of solution. The direction and the scanning rates of the stresses is the same for the different curves making up a figure. The magnitude of the complex viscosity $|\eta^*(\omega)|$, the storage modulus G' and the loss modulus G'' were measured generally in an angular frequency range between $\omega = 0.1$ and $\omega = 250$ rad/s^{-1}.

Results and discussion

Zero shear viscosity η_0

Figure 2 gives the zero shear viscosity for the 0.3 M/l solution of CTAB against the concentration C_s of salt $NaNO_3$ at 30 °C. 0.3 M/l is the concentration of CTAB alone corresponding approximately to the sphere to rod transition. In the domain of salt content studied here, the viscosity η_0 shows a pronounced maximum as a function of salt concentration. This curve, for reasons given later, is decomposed into three parts (A), (B), (C) corresponding to increasing salt [$NaNO_3$] concentration. It is well known that aqueous ionic solutions of surfactants can undergo uniaxial growth upon addition of salt, the consequence being an increase in the viscosity of the solution. We can see in Fig. 2 that for a fixed concentration C_D of the surfactant of 0.3 M/l, the first part of the curve effectively corresponds to an increase of the zero shear viscosity when the concentration of the salt increases. It is generally admitted that increasing the salt concentration amounts to increasing the curvature energy of surfactant molecules in the end-cap relative to the one in the cylindrical body of the micelle. This leads to an increase in micellar length (and hence in the zero-shear viscosity). The decrease in the viscosity for $C > C_{max}$ cannot be accounted for by the reptation-reaction model of Cates. It was suggested that the high fluidity observed with high content of the added salt is associated with the formation of crosslinks between micelles by fusion [12]. So, we obtain in such a situation, a solution of branched micelles. A recent model [13] shows that in this situation, the zero-shear viscosity is reduced with respect to entangled micellar solutions obtained for less salt concentration solutions. The explanation given is that for high salt concentration, the obtained connections can move along the cylindrical part of the micelle. In the limit of numerous connections, the micelles can form a saturated network, totally multiconnected.

Fig. 2 Variation of the zero-shear viscosity versus salt concentration: [CTAB] = 0.3 M/l, $T = 30$ °C

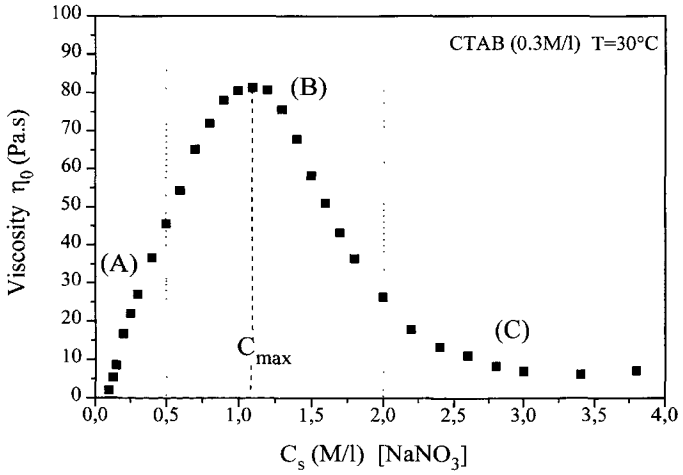

Salt effect

Linear behaviour in the domains (A), (B) and (C)

Theoretically (Cates' model), it is predicted that if $\tau_b \ll \tau_{rep}$ we can observe an almost monoexponential stress decay with a relaxation time τ_R given by $\tau_R = (\tau_b \tau_{rep})^{1/2}$. So the stress relaxation function is $G(t) = G_0 e^{-t/\tau}$. In such a situation, the simplest model that can describe the behaviour of the viscoelastic solution is the Maxwell model. It consist of a spring (of shear modulus G_0) and a dashpot (which corresponds to the constant viscosity η_0) connected in series. The linear dynamic properties of this Maxwell element correspond to linear differential equations. The solutions for G' (the storage modulus), G'' (the loss modulus) and $|\eta^*|$ (the complex viscosity) are

$$G'(\omega) = G_0 \frac{\omega^2 \tau_R^2}{1 + \omega^2 \tau_R^2},$$

$$G''(\omega) = G_0 \frac{\omega \tau_R}{1 + \omega^2 \tau_R^2}$$

and

$$|\eta^*|(\omega) = \frac{\eta_0}{\sqrt{1 + \omega^2\tau_R^2}} .$$

So, dynamic measurements in the range of linear viscoelasticity yield informations on the structure at rest. G_0 is correlated to the degree of entanglements of the network. In Fig. 3, we have represented the evolution of G_0 as a function of the salt concentration. In this curve, we can see approximately the three domains, previously defined by (A), (B) and (C). In the same figure, we show the evolution of τ_R, the terminal relaxation previously defined and which characterize the network dynamics. As we can see, this curve exhibits a pronounced maximum for $C_s \approx 1.1$ M/l. Values of G_0 and τ_R given in this figure are obtained by fitting $G'(\omega)$ and $G''(\omega)$ with the relations given above. In Fig. 4, the data are presented for three salt concentrations under the form of a Cole–Cole plot ($G'' = f(G')$). In this representation, a perfect Maxwell model gives a half circle. For the three concentrations, we obtain deviation from half circle in the high frequency range, in particular due to the Rouse modes. In this Fig. 4 it can be easily seen that it is for the highest concentration of $NaNO_3$ that the agreement with the Maxwell model is the best one, where the turn occurs for the greatest ω. This linear rheological study allows us to obtain a value of the entanglement length l_e by [14–16]

$$G'_\infty = G_0 = \frac{k_B T}{l_e^{9/5}} .$$

In addition, the ratio G''_{min}/G_0 can be identified with $l_e/\bar{L}$ [17] if this ratio is small enough (≤ 0.1) (we will see in the next figure that it is the case).

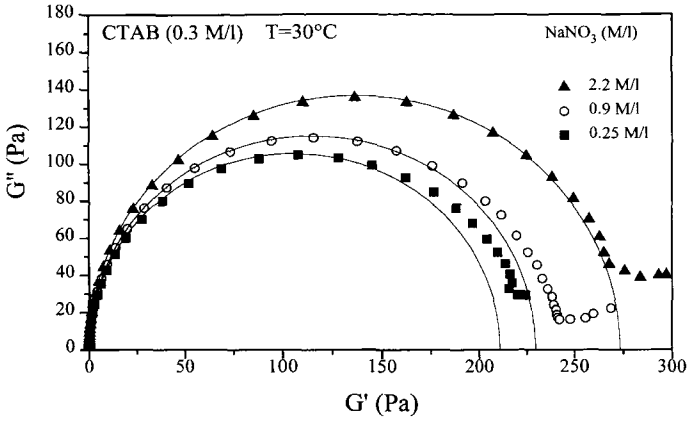

Fig. 4 Experimental Cole–Cole plot $G'' = f(G')$ for different salt concentrations. The lines correspond to the osculating semi-circles at the origin (best fit). [CTAB] = 0.3 M/l, $T = 30\,^\circ C$

From these relations, in Fig. 5 we have represented the evolution of $\bar{L}$, the apparent average micellar length and l_e, the entanglement length, with variable concentrations of the added salt.

The $\bar{L}$ curve also exhibits a pronounced maximum for $C_s \approx 1.1$ M/l. It is generally admitted that for a fixed surfactant concentration, a rise of salt content, as a consequence of the screening of electrostatic interactions, induces a micellar growth. As expected, in the first part of the curve of Fig. 5, $\bar{L}$ is an increasing function of [$NaNO_3$] concentration. The $\bar{L}(C_s)$ curve is close to the $\eta_0(C_s)$ curve. For the two curves, the maximum is obtained practically for the same C_s, around 1.1 M/l. The decreasing part of the $\eta_0(C_s)$ curve was explained previously by the possibility that an excess of salt could lead to a branching of the

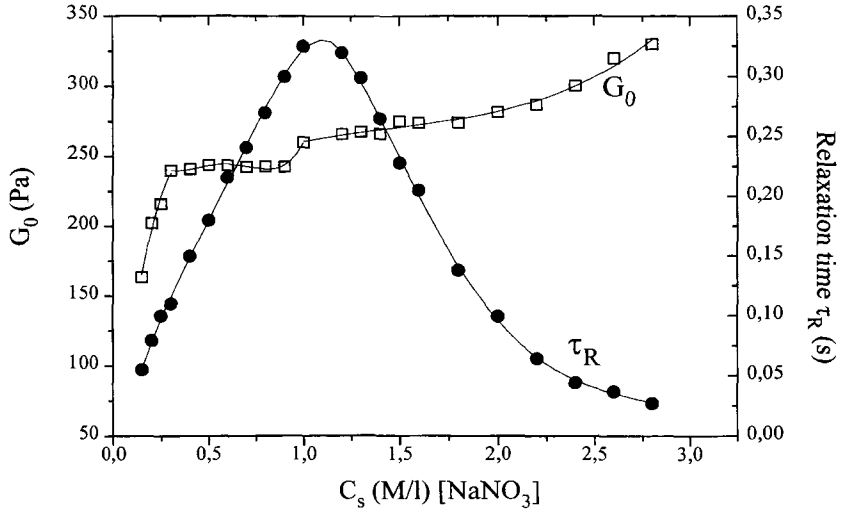

Fig. 3 Variation of the plateau modulus G_0 and the terminal relaxation time τ_R versus salt concentration: [CTAB] = 0.3 M/l, $T = 30\,^\circ C$

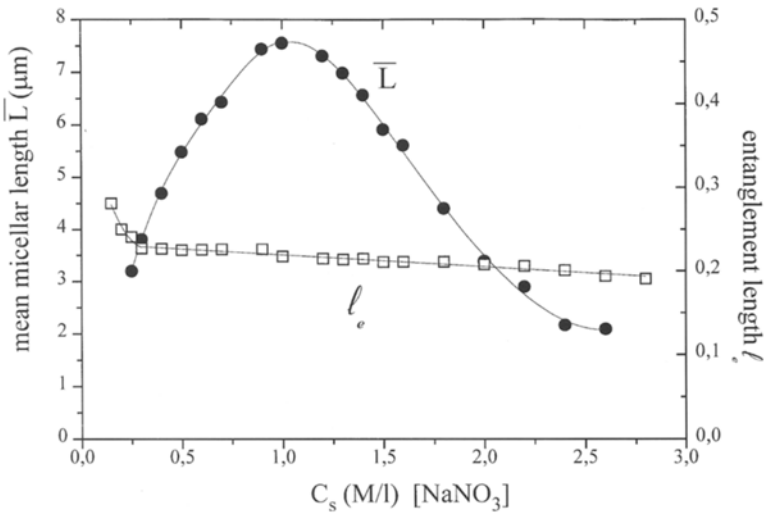

Fig. 5 Apparent mean micellar length and entanglement length as a function of salt concentration: [CTAB] = 0.3 M/l, $T = 30\,^{\circ}C$

micelle. The same phenomenon can explain the decreasing of $\bar{L}$, this quantity now having a new meaning corresponding to an apparent average length. We notice that the maximum of the $\tau_R(C_s)$ curve also corresponds approximately to the same value of C_s. It is obvious that the connections between thread-like micelles profoundly affect the relaxation of the system. The reptation process of branched micelles was studied theoretically by Lequeux [13]. It leads to a predicted reduction of the zero-shear viscosity η_0 and of its surfactant concentration dependence [12]. It is mentioned that all the results concerning the rheology of linear worm-like micelle (without connections) can be applied to a system with branched micelles by $\bar{L}_e$, taking the place of $\bar{L}$ the new distance being the harmonic mean between the average distance from one point along the micelle to the first cross-link and the average distance from that point to the first end-cap. If the micelles are branched, no qualitative change in the shape of the Cole–Cole plots are expected.

The decreasing part of the τ_R curve could also be explained, in the model of sliding connections, by the predicted strong increase in the reptation diffusion [13]. In the Fig. 5 we can see that despite the pronounced maximum in the $\bar{L}(C_s)$ curve, the entanglement length l_e remains practically constant in all the range of salt concentration studied here.

Non-linear behaviour of CTAB/$NaNO_3$ system at a fixed concentration $C_D = 0.3$ M/l of surfactant

The non-linear rheological response of the aqueous CTAB/$NaNO_3$ system to shear flow is given in Figs. 6, 7 and 8 for many concentrations of $NaNO_3$ (at $T = 30\,^{\circ}C$)

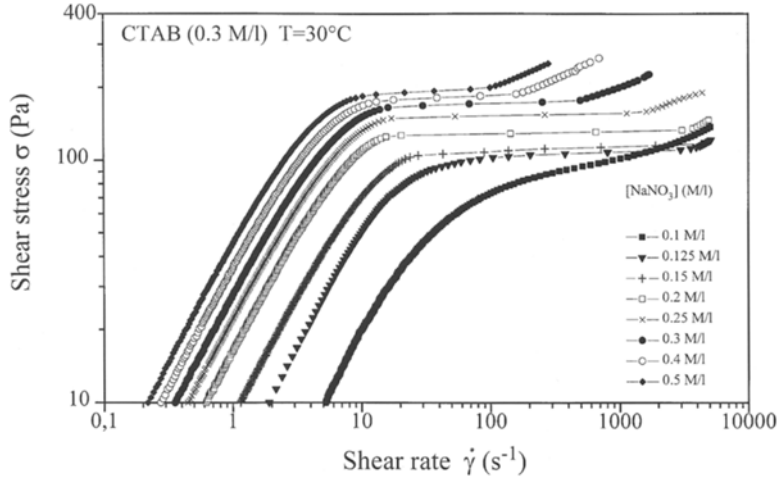

Fig. 6 Variation of the shear stress versus shear rate for solutions at [CTAB] = 0.3 M/l, $T = 30\,^{\circ}C$ and different salt concentrations between 0.2 and 0.5 M/l

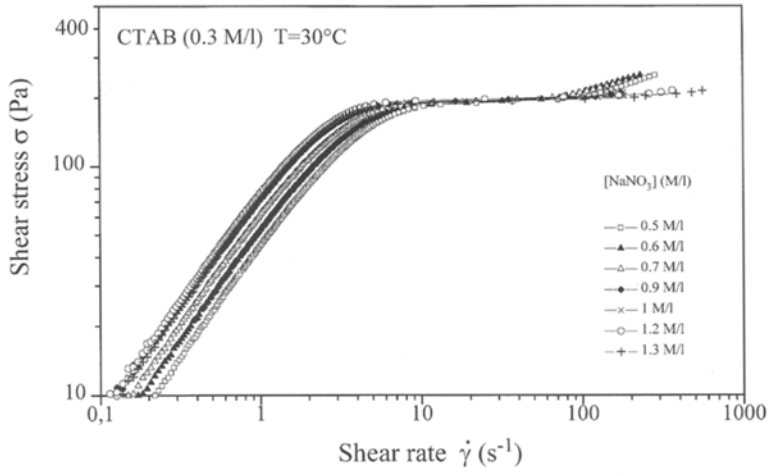

Fig. 7 Variation of the shear stress versus shear rate for solutions at [CTAB] = 0.3 M/l, $T = 30\,^{\circ}C$ and different salt concentrations between 0.5 and 1.3 M/l

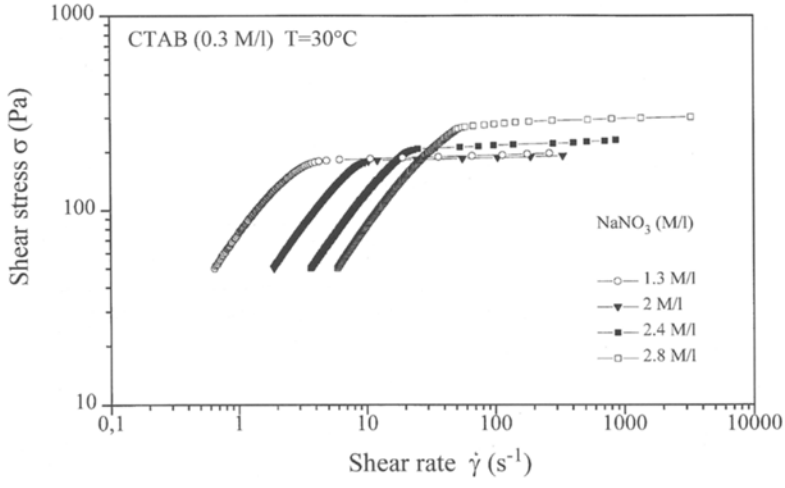

Fig. 8 Variation of the shear stress versus shear rate for solutions at [CTAB] = 0.3 M/l, $T = 30\,^{\circ}C$ and different salt concentrations between 1.3 and 2.8 M/l

in the three domains (A), (B), and (C) defined before. Figure 6 shows the evolution of the shear stress σ as function of the shear rate $\dot{\gamma}$ for various $NaNO_3$ concentrations lying between 0.1 and 0.5 M/l ($= C_A$), i.e., for the domain (A). It is interesting to notice that for these small salt concentrations, the CTAB/$NaNO_3$ system clearly exhibits the three domains (I), (II) and (III) schematically defined in Fig. 1. Several important points can be noted. In the first domain (A), for sufficiently high salt concentration, the $\sigma = f(\dot{\gamma})$ curves exhibit a plateau (II) at $\sigma = \sigma_c$ for $\dot{\gamma} = \dot{\gamma}_{1c}$. The steady shear behaviour of the worm-like surfactant solution is remarkable. Above this critical shear rate, the shear stress becomes roughly independent of $\dot{\gamma}$. This region of constant shear stress is very reproducible. We can notice that with this surfactant system and the range of shear rate accessible, for $\dot{\gamma}$ greater than the second critical value $\dot{\gamma}_{2c}$, we can observe the domain (III) showing a new increase of the shear stress. At these high shear rates, contrary to the results mentioned in [18], for example, the experiments, in the domain (A), are possible to perform. The material is not expelled from the rheometer gap.

The plateau value $\sigma = \sigma_c$ and the corresponding domain (II), in log–log representation of $\eta(\dot{\gamma})$ correspond to the linear decreasing of the viscosity with a characteristic slope of -1. In the (III) domain, the slope, in the same representation is nearly -0.4, practically independent of the salt concentration. The evolution of the created structure obtained for shear rate $\dot{\gamma} > \dot{\gamma}_{2c}$ appears only slightly influenced by salt concentration. We can also notice that in the domain (A), σ_c increases with salt concentration whereas the critical shear rate $\dot{\gamma}_{1c}$ decreases. The evolution of these two rheological parameters is correlated to the growing size of the micelles in the domain (A). Longer the micelles, easier is their alignment in the shear flow. So, logically $\dot{\gamma}_{1c}$ is a decreasing function of salt concentration. $\dot{\gamma}_{1c}$ corresponds to the beginning of the stress plateau. The

transition from the (linear) domain (I) to the plateau is smoother than that obtained for the concentrated system, near the concentration corresponding to the static transition giving a liquid crystal system [19, 20]. In the situation of Fig. 6, the rounded curve at the transition means that before the true transition these exists a progressive alignment of the micelles in the shear rate.

The end of the stress plateau and the new increase in the shear stress correspond to a second characteristic shear rate $\dot{\gamma}_{2c}$ which is strongly dependent on the salt concentration. The more important the salt is, the lesser is the value of $\dot{\gamma}_{2c}$. The quantity $\Delta\dot{\gamma}_c = \dot{\gamma}_{2c} - \dot{\gamma}_{1c}$ is a characteristic of the importance of the plateau. We can see that $\Delta\dot{\gamma}_c$ decreases with increasing salt concentration. The second transition (II) → (III) is such a strong function of the amount of added salt and that it is a function of the length of the micelles too. The greater the micelles, the smaller the value of critical $\dot{\gamma}_{2c}$. At the difference of concentrated solution without salt [19], the third domain (III) does not superpose for the different salt contents. We can also see that for smaller concentrations (for example 0.1 M/l in Fig. 6), $\sigma = f(\dot{\gamma})$ shows a smooth evolution without well characterizing broken line and plateau of the shear stress. The domain (III) is also badly defined. In the concentration range $0.5\ \text{M/l} \leq C_s \leq 1.3\ \text{M/l}$ ((B) domain), the flow curves of Fig. 7 taken seperately have great similarities with those of Fig. 6, but a fundamental difference is that the critical shear stress σ_c is independent of the salt concentration ($\sigma_c \approx 195$ Pa). In this domain (B) it is experimentally difficult to obtain the domain (III) of the flow curve for all salt concentrations. At high shear rate, slipping can occur giving no reproducible and inexploitable results. Curves of Fig. 7 seem to indicate that the induce structure for $\dot{\gamma} > \dot{\gamma}_{1c}$ is here independent of the salt concentration and is induced under the same critical shear stress σ_c. In Fig. 8, we have given the results for the high salt concentration (domain (C)). For $C_s > 2$ M/l, σ_c is, as in domain (A), an increasing function of C_s. The transition between domains (I) and (II) also become more abrupt. This behaviour of the stress plateau is also obtained for concentrated surfactant solutions near a nematic phase at rest [19–21]. In this third domain (C) of salt concentration for practical reasons it is not possible to observe reproducibly and without degradation the domain (III) of the flow curve.

Comparison between experimental results and Cates' theory

One of the main purpose of this paper is to relate the predictions of Cates et al. [10] concerning the non-linear rheological behaviour of the micellar solutions to experimental results obtained with entangled worm-like micellar

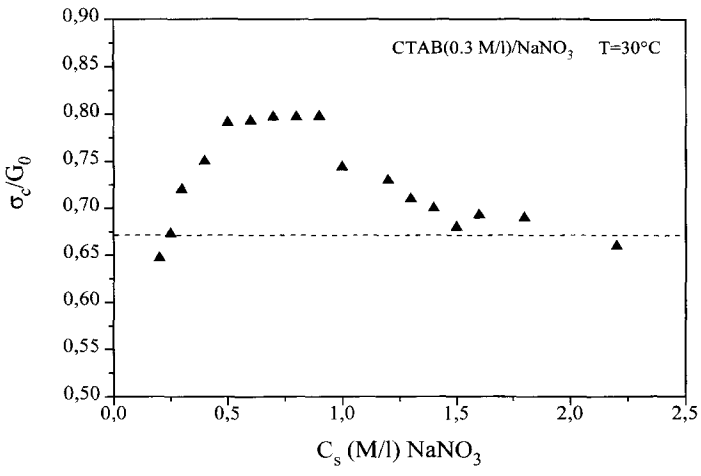

Fig. 9 Variation of the ratio σ_c/G_0 versus salt concentration: [CTAB] = 0.3 M/l, $T = 30\,^{\circ}\text{C}$

solutions. Using results given in Figs. 6–8 to obtain σ_c and Fig. 3 for G_0 we have, in Fig. 9, given the evolution of the ratio σ_c/G_0 against salt concentration. It can be noticed that this ratio is not too far from the theoretical predicted value of 0.67, the deviation here being the most pronounced in the domain of salt concentration in which the micellar length is growing, and for which a value of ≈ 0.8 is obtained. It is for concentrations C_s greater than 1.1 M/l, in the decreasing domain of variation of the apparent mean length $\bar{L}$ that the ratio σ_c/G_0 is closer than the theoretical value. In this domain, it is expected that the system is multiconnected, but we have seen in Fig. 4 that it is in this domain of salt content that the system shows the best Maxwellian behaviour (monoexponential).

As the model of Cates et al. is meant for the case where the stress relaxation function is close to monoexponential, the evolution of Fig. 9 for high salt concentration is not surprising, but explanation of complete evolution (and values obtained) is still lacking.

We can see in Fig. 10 that the critical parameter $\dot{\gamma}_{1c}$, predicted by the theory to be equal to $2.6/\tau_R$, shows immediate difference with this value. Contrary to the comparison of σ_c/G_0 with the predicted value 0.67, in this case, it is for $C_s = 1$ to 1.1 M/l, e.g. near the maximum of the $\eta_0(C_s)$ curve that the coincidence is the best. The divergence between the two values of $\dot{\gamma}_{1c}$ and $2.6/\tau_R$ increased when the salt concentration increases for $C_s > 1.1$ M/l. It seems that, for this parameter, the appearance of the multiconnected network deeply affects the results. This is not unexpected, because the meaning of τ_R in this case is not the one taken into account by the Cates' theory. To conclude, we can notice that nowadays, the existence of a plateau in $\sigma(\dot{\gamma})$ behaviour at a level $\sim 0.67 G_0$ has only been reported in few cases, e.g. in CPCl/Sal (cetylpyridinium

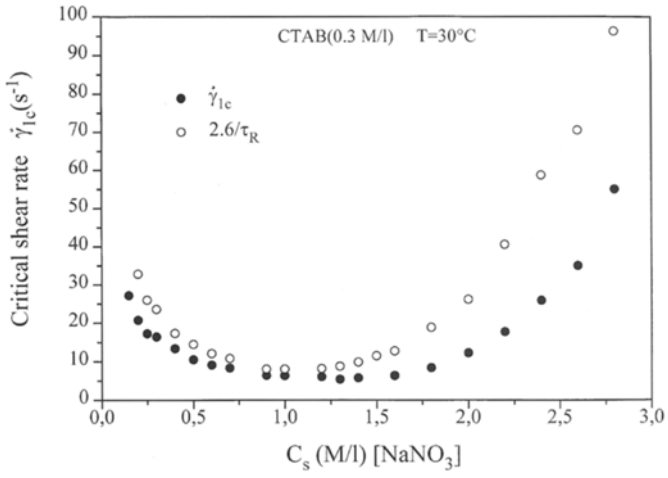

Fig. 10 Variation of the experimental value of the critical shear rate $\dot{\gamma}_{1c}$ and of $2.6/\tau_R$ versus salt concentration: [CTAB] = 0.3 M/l, $T = 30\,°C$

chloride with sodium salicylate in water) by Rehage and Hoffmann [22], approximately in CTAB/KBr at high salt contents [12], $CPClO_3/NaClO_3$ [17] and by Berret in CPCl/Sal [23]. Agreements of $\dot{\gamma}_{1c}$ and $2.6/\tau_R$ have not been reported in publications to our knowledge.

Surfactant concentration effect

Linear behaviour

Again, to obtain information about the system at rest, we have performed dynamical measurements in the linear domain for a fixed salt concentration of 0.3 M/l. Usually, an increase of G_0 (the shear modulus) is predicted with increasing detergent concentrations for giant micelles system. This evolution can be seen in Fig. 11 in the Cole–Cole representation: the diameter of the osculator circle at the origin is increasing with C_D, with an increasing departure from the half circle at high frequencies. This behaviour is consistent with observations of Khatory [6] for the CTAB/KBr system. The dynamical measures in the linear range allows us to obtain η_0, τ_R and G_0. We found here (Fig. 12) in function of the surfactant concentrations C_D:

$$\eta_0 \sim C_D^{2.63}, \quad \tau_R \sim C_D^{0.86}, \quad G_0 \sim C_D^{1.86}.$$

Theoretically, it is predicted that for $\tau_b \ll \tau_{rep}$

$$\eta_0 \sim C_D^{3.5}, \quad \tau_R \sim C_D^{5/4} \text{ and } G_0 \sim C_D^{9/4}.$$

We can notice that all the experimental exponents obtained are smaller than predicted. Experimental results on CTAB/KBr system in [6] also give 2.42 and 1.85 respectively for η_0 and G_0 with similarities with those obtained with the CTAB/$NaNO_3$ system studied here. In the work [6] the salt concentration is fixed equal to 1.5 M/l. In ours it is only 0.3 M/l. The obtained results suggest that $NaNO_3$ is more efficient than KBr, in its screaning effect and to obtain a multiconnected system.

The smallest predicted exponent corresponding to η_0 as to G_0 can be partly explained [6], for the former by the fluidizing effects of the connections between the micelles and for G_0 by the fact that the connections in micellar system are less effective than entanglements in solutions.

Non-linear behaviour at fixed salt concentration $C_s = [NaNO_3] = 0.3\ M/l$

We have also studied in the non-linear domain the effect of the surfactant concentration on the rheological behaviour of the micellar solutions of CTAB/$NaNO_3$ for a fixed salt concentration of 0.3 M/l. In Fig. 13 we have represented the evolution of the shear stress σ against shear rate $\dot{\gamma}$ at $T = 30\,°C$ for eight surfactant concentrations, lying

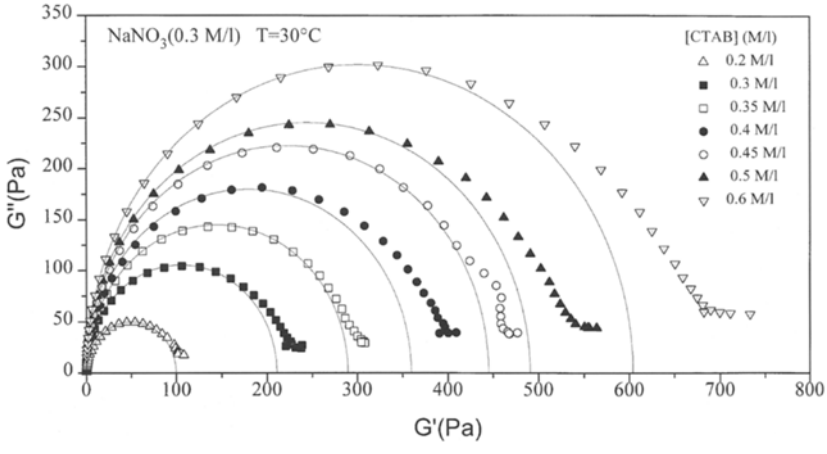

Fig. 11 Experimental Cole–Cole plot $G'' = f(G')$ for different surfactant concentrations. The lines correspond to the osculating semi-circles at the origine (best fit). [$NaNO_3$] = 0.3 M/l, $T = 30\,°C$

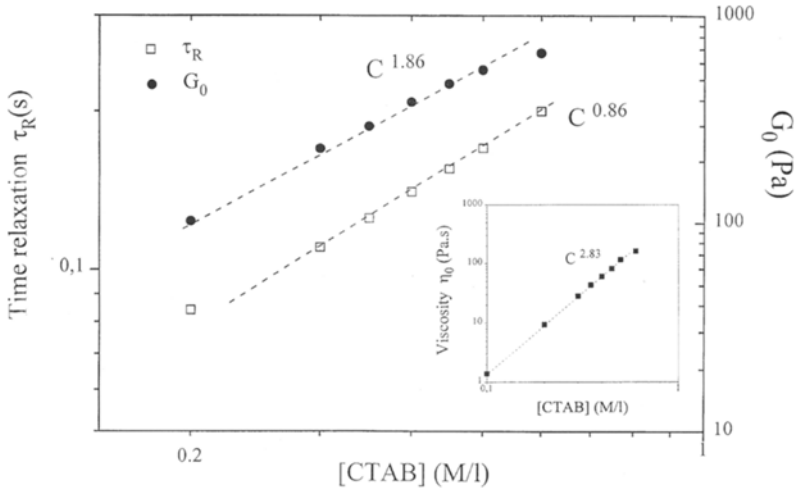

Fig. 12 Experimental log–log representation of G_0 (plateau modulus), τ_R (terminal relaxation time) and η_0 (zero-shear viscosity) as a function of surfactant concentration: $[NaNO_3] = 0.3$ M/l, $T = 30$ °C

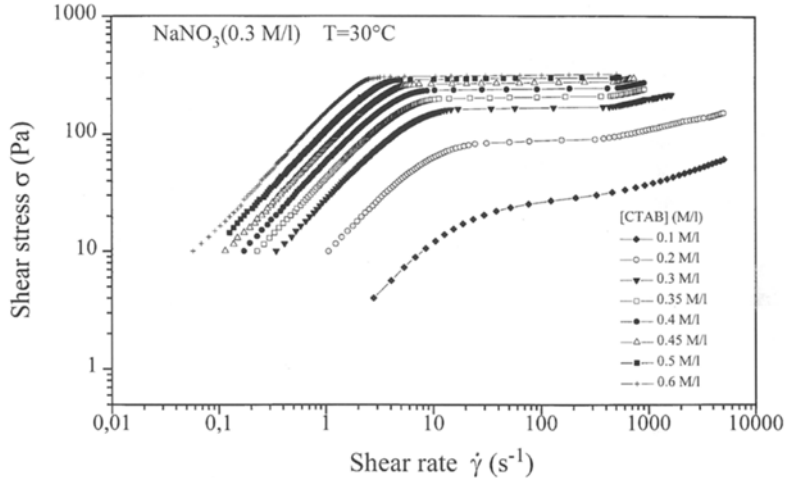

Fig. 13 Variation of the shear stress versus shear rate for solutions at $[NaNO_3] = 0.3$ M/l, $T = 30$ °C and different surfactant concentrations between 0.1 and 0.6 M/l

between 0.1 and 0.6 M/l. We can see that for each curve of the figure, qualitatively, the evolution is similar as in Fig. 6. The plateau value of the shear stress σ_c increases with the surfactant concentration with a trend of saturation of the order of 315 Pa corresponding to the highest CTAB concentration studied here. The more important the surfactant concentration C_D, the sharper is the transition between the domains (I) and (II). The value of $\dot{\gamma}_{2c}$ above, which is the III domain is very slightly sensitive to C_D. The slope in this domain, in the log–log representation of $\eta(\dot{\gamma})$ is about -0.4 (when the domain exists distinctly). The smallest concentration (0.1 M/l) of CTAB studied here no more gives a plateau of the shear stress, but a pseudo-third domain appears with a different slope. Contrary to Fig. 6, with increasing C_D we observe an increase of $\Delta\dot{\gamma}$, the length of the shear stress plateau. The dependence of $\dot{\gamma}_{1c}$ on C_D is also more pronounced than on C_s. Experiences with Small-Angle Neutrons Scattering (SANS) [24] on CTAB/KBr (1.5 M/l) show that orientations of micellar chain are only present when $\dot{\gamma} > \dot{\gamma}_{1c}$. These experimental results and others with optical observations [23, 25, 26] confirm that for $\dot{\gamma}_{1c} \leq \dot{\gamma} \leq \dot{\gamma}_{2c}$, the shear stress is a constant throughout the sheared material but that two shear rates (a high and a low) can coexist. In such a situation, as theoretically predicted [10] the flow takes a banded form with volume fractions arranged to match the macroscopic shear rate $\dot{\gamma}$ externally applied to the solution.

Comparison between experimental results and Cates' theory

In Fig. 13 we can notice that σ_c increases (as G_0) with the surfactant concentration. In Fig. 14 we have reported the evolution of σ_c/G_0 as a function of C_D. This ratio is a decreasing function. The Cole–Cole of Fig. 11 shows that it

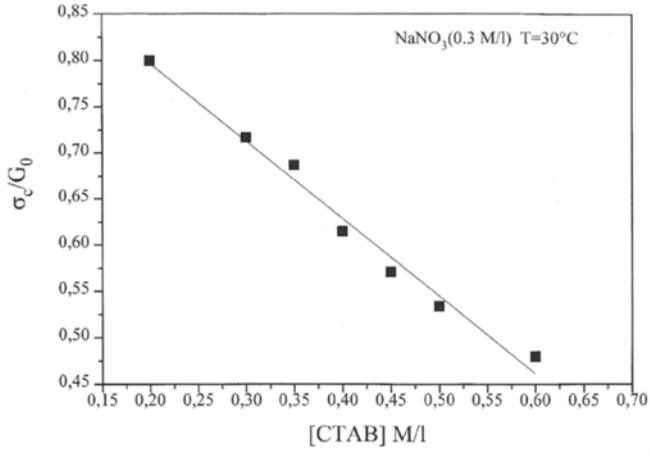

Fig. 14 Evolution of the ratio σ_c/G_0 versus surfactant concentration: $[NaNO_3] = 0.3$ M/l, $T = 30\,^{\circ}C$

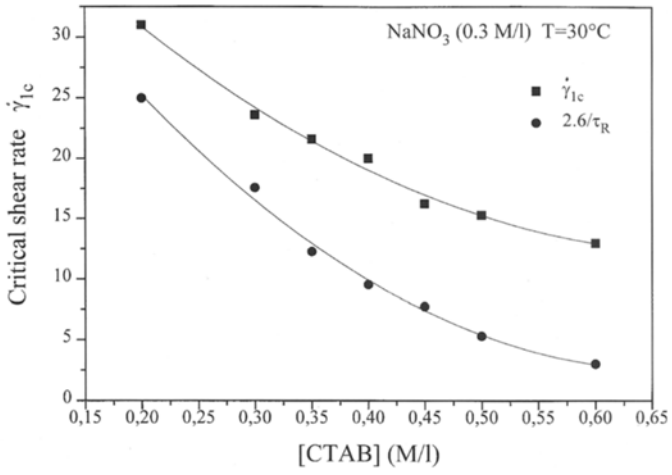

Fig. 15 Variation of the experimental value of the critical shear rate $\dot{\gamma}_{1c}$ and $2.6/\tau_R$ versus surfactant concentrations: $[NaNO_3] = 0.3$ M/l, $T = 30\,^{\circ}C$

is for a surfactant concentration of around 0.35 M/l (C_s being fixed at 0.3 M/l) that the deviation from the half circle comes later and is less pronounced. In this situation, the relaxation function is nearly a monoexponential and we can see in Fig. 14 that in this case σ_c/G_0 is very near the theoretical expected value of 0.67. This suggests that, as theoretically predicted, it is necessary to have a Maxwellian behaviour to obtain correct expected effects. The observed deviations giving smaller values than 0.67 for the greatest concentrations of the surfactant can be related to the nature of concentrated system obtained in that situation, the processes of relaxation being modified, leading to discrepancy with the theoretical expected values. In Fig. 15 we have represented the evolution of $\dot{\gamma}_{1c}$ and $2.6/\tau_R$ as a function of CTAB concentration. In this curve we can also note that the deviation between the two values rises with C_D, the agreement appearing to be the best for small concentration of CTAB, but if C_D is too small we do not have entangled worm-like micellar solution. The non-coincidence of $\dot{\gamma}_{1c}$ and $2.6/\tau_R$ observed experimentally is normal. A phenomenon of nucleation could be the cause of this disagreement [23].

Temperature effect on the $\sigma = f(\dot{\gamma})$ curves

Figures 16, 17 and 18 represent typical experimental results obtained for the $\sigma(\dot{\gamma})$ curves at different temperatures. Curves in Fig. 16 correspond to the domain (A) of concentration $NaNO_3$, in Fig. 17 to the domain (B), for $C_s < C_{max}$ and, in Fig. 18 for a salt concentration superior to C_{max}. These figures are interesting for they show the progressive evolutions of the flow curves. In the intermediate range

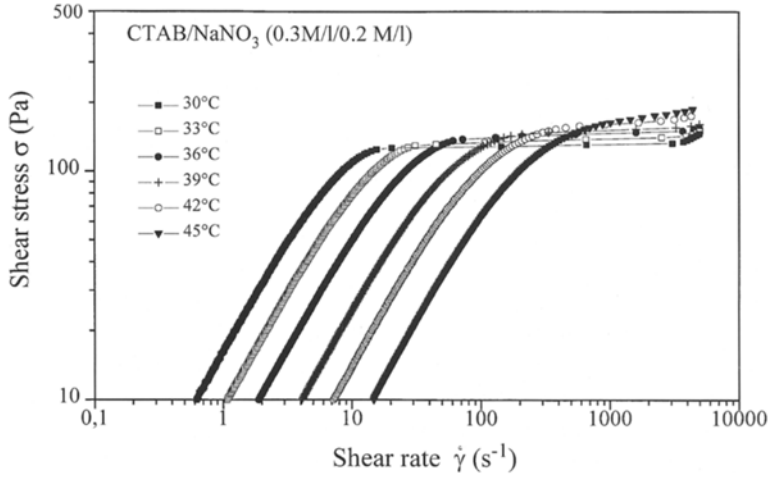

Fig. 16 Variation of the shear stress versus shear rate for solutions at [CTAB] = 0.3 M/l, $[NaNO_3] = 0.2$ M/l and different temperatures between 30 and 45 °C

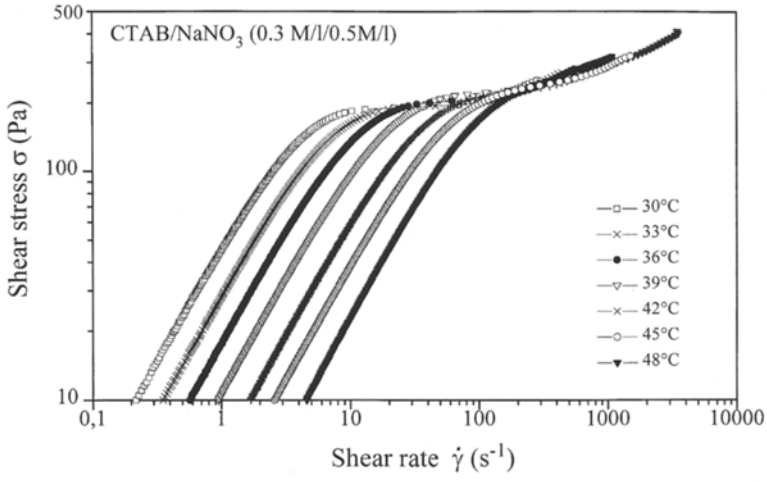

Fig. 17 Variation of the shear stress versus shear rate for solutions at [CTAB] = 0.3 M/l, [$NaNO_3$] = 0.5 M/l and different temperatures between 30 and 48 °C

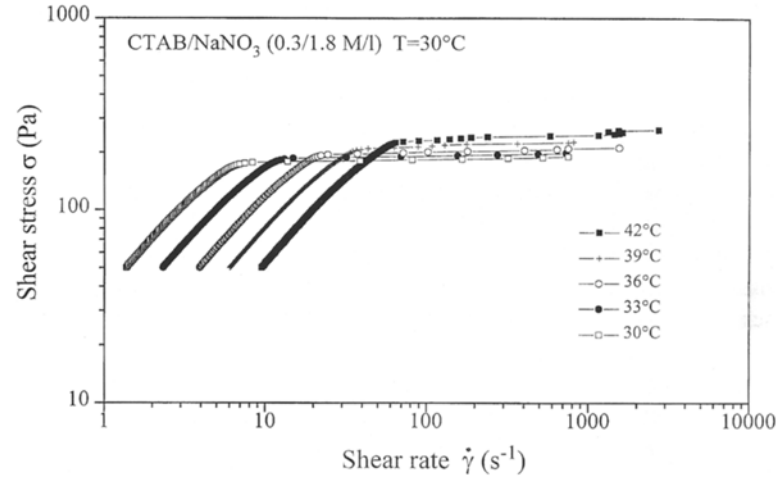

Fig. 18 Variation of the shear stress versus shear rate for solutions at [CTAB] = 0.3 M/l, [$NaNO_3$] = 1.8 M/l and different temperatures between 30 and 42 °C

concentration of the salt (Fig. 17) the plateau domain (II) of the flow curves practically disappears (giving a kind of pseudo-plateau or an inflection point in the curve). We can also note that the transitions at $\dot{\gamma}_{1c}$ between the (I) and (II) domain are sharper in the presence of high salt concentration. It is well known that the apparent average micellar length $\bar{L}$ decreases when the temperature increases. We have the relation

$$\bar{L} \sim \phi^{1/2} \exp(E_{scis}/2k_B T) ,$$

where ϕ is the surfactant volume fraction and E_{scis} the scission energy of the micelle. The smaller the micelles greater the critical gradient necessary to orient the particles, and more progressively should this transition occur. This is in agreement with experimental results presented in Figs. 16–18, $\dot{\gamma}_{1c}$ increasing with the temperature and the transition in the flow curve being more rounded with the rising temperature (except in Fig. 18 for high salt concentration). When a plateau of shear stress exists, its value is a function of the temperature. We can notice that after the pseudoplateau (Fig. 17) for the system CTAB (0.3 M/l)/$NaNO_3$ (0.5 M/l) all the curves practically converge to approximately the same one, independent of the temperature. This agreement means that the viscosity of the induced phase in the pseudo-domain (III) is little influenced by the temperature as are the crystalline phase of the nematic type, for example [20].

Conclusion

In theoretical studies of the non-linear rheology of worm-like micellar solutions, it was often said that it was a lack of complete experimental results concerning this problem. The aim of this experimental work was to give for a classical surfactant system, the CTAB and also a salt, the less frequently used $NaNO_3$, a set as complete as possible of characteristic values concerning this system. From an

experimental point of view, it was found that this system is interesting for different reasons, an important one being that with it, it is possible to study the rheological properties of solutions up to high values of the shear rate (e.g. $\dot{\gamma}_{2c}$) without instabilities leading to expulsion from the device [20, 27]. So in this work we have presented experimental results often showing distinctly the critical shear rates $\dot{\gamma}_{1c}$ and $\dot{\gamma}_{2c}$ characterizing, respectively, the beginning and the end of the predicted shear stress plateau (at a level σ_c). For shear rates included between the two critical shear rates exists a shear banding structure. For surfactant concentrations close (but inferior) to the one at rest giving a transition to a nematic phase, the nature of the obtained shear banding structure is now relatively clear [27]: a shear-induced isotropic to nematic phase transition of the first order occurs under flow. The nematic strate is submitted to a high shear, the "isotropic" one to the lower shear, the two being submitted to the same shear stress σ_c.

For lower surfactant concentrations the mechanism of the shear banding structure is less clear. Theoretically, it is interpreted in terms of a pure mechanical instability of the shear banding type.

In this work, we have investigated the influence of the surfactant and salt concentrations and of the temperature on the flow curves. The obtained results were compared to the theoretical predictions of Cates et al. regarding, in a banding structure, the relations between $\dot{\gamma}_{1c}$, σ_c, τ_R (the terminal relaxation time) and the Maxwellian character of the solutions. If in some cases, good or acceptable agreements can be found with theoretical predictions, some theoretical efforts must be still done to explain all the results obtained. Simultaneously, other experimental techniques such as SANS, flow birefringence, must be used to understand completely the true nature, in all cases, of the shear banding structure appearing for sufficiently high shear in worm-like micellar solutions.

References

1. Candau SJ, Hirsch E, Zana R (1985) J Colloid Interface Sci 105:521–528
2. Candau SJ, Hirsch E, Zana R, Adam (1988) J Colloid Interface Sci 122: 430–440
3. Candau SJ, Hirsch E, Zana R (1984) J Phys (Paris) 45:1263–1270
4. Candau SJ, Hirsch E (1989) Langmuir 5:1225–1229
5. Porte G (1982) Thèse de Doctorat d'Etat, Université de Montpellier, unpublished
6. Khatory A (1993) Thèse de Doctorat, Université de Strasbourg, unpublished
7. Larsen JW, Magid LJ (1974) J Am Chem Soc 96:5774
8. Cates ME (1990) J Phys Chem 94: 371–375
9. Makhloufi R, Decruppe J-P, Aït-ali A, Cressely R (1995) Europhys Lett 32: 253–258
10. Spenley NA, Cates ME, McLeish TCB (1993) Phys Rev Lett 71:939–942
11. Makhloufi R, Cressely R (1990) Colloid Polym Sci 270:1035–1041
12. Khatory A, Lequeux F, Kern F, Candau SJ (1993) Langmuir 9:1456–1464
13. Lequeux F (1992) Europhys Lett 19: 675–681
14. Doi D, Edwards SF (1986) The Theory of Polymer Dynamics. Clarendon Press, Oxford
15. Cates ME, Macromolecules (1987) 20:2289–2296
16. Turner MS, Cates ME (1991) Langmuir 7:1590–1594
17. Granek R, Cates ME (1992) J Chem Phys 96:4758–4767
18. Callaghan PT, Cates ME, Rofe CJ, Smeulders JBAF (1996) J Phys II France 6:375–393
19. Berret J-F, Roux DC, Porte G, Lindner P (1994) Europhys Lett 25:521–526
20. Cappelaere E, Cressely R, Decruppe J-P (1995) Coll Surf 104:353–374
21. Schmitt V, Lequeux F, Pousse A, Roux D (1994) Langmuir 10:955–961
22. Rehage H, Hoffmann H (1991) Molec Phys 74:933–973
23. Berret JF, Roux D, Porte G (1994) J Phys II France 4:1261–1279
24. Schmitt V (1994) Thèse de Doctorat, Université de Strasbourg, unpublished
25. Decruppe J-P, Cressely R, Makhloufi R, Cappelaere E (1995) Colloid Polym Sci 273:346–351
26. Berret J-F, Porte G, Decruppe J-P (1996) Phys Rev E, to be published
27. Cappelaere E, Berret J-F, Decruppe J-P, Cressely R, Lindner P (1996) to be published
28. Doi M, Edwards SF (1979) J Chem Soc Faraday Trans 274:1709–1802–1818